Proc. 29th Int. Workshop on Vertex Detectors (VERTEX2020)
JPS Conf. Proc. **34**, 010016 (2021)
https://doi.org/10.7566/JPSCP.34.010016

First prototype of finely segmented HPK AC-LGAD detectors

Koji Nakamura[1], Sayuka Kita[2], Tatsuki Ueda[3], Kazuhiko Hara[4] , and Hisanori Suzuki[3]

[1]*Institute of Particle and Nuclear Studies, High Energy Research Organization, 1-1 Oho, Tsukuba, Ibaraki, 305-0801, Japan*
[2] *College of Physics School of Science and Engineering, University of Tsukuba, 1-1-1 Tennodai, Tsukuba, Ibaraki, 305-8571, Japan*
[3] *Graduate School of Physics Pure and Applied Sciences, University of Tsukuba, 1-1-1 Tennodai, Tsukuba, Ibaraki, 305-8571, Japan*
[4] *Faculty of Pure and Applied Sciences and Tomonaga Center for the History of the Universe, University of Tsukuba, 1-1-1 Tennodai, Tsukuba, Ibaraki, 305-8571, Japan*

E-mail: Koji.Nakamura@cern.ch

(Received December 11, 2020)

The presentation describes the development of a silicon detectors for high energy particle physics experiments, focusing on detectors that can provide fast timing capabilities with fine spatial resolutions. The Low Gain Avalanche Diode (LGAD) sensors fabricated by Hamamatsu Photonics (HPK) have shown to achieve a 30 ps time resolution for a larger (millimeter scale) pad type electrode detector. To realize a sensor with a spatial resolution suitable for particle tracking with a high fill factor, development of LGAD detectors with AC-coupled electrodes (AC-LGAD) is carried out by KEK/Tsukuba HPK. In this paper, performance of first AC-LGAD prototypes, pad type detector and finely stripped detector, will be presented.

KEYWORDS: Silicon, tracker, LGAD, AC-LGAD

1. Introduction

This paper describes the development of silicon detectors suitable for high energy particle physics experiments, focusing on 4-dimensional (time and space) detectors that can provide a fast timing capability and fine spatial resolution. Particle detectors at future lepton or hadron colliders will require very large area trackers, e.g. reaching or exceeding 1000 m^2 while maintaining a micron-level spatial resolution. A timing capability of O(10) ps in addition should allow reconstructing particles from primary collisions efficiently. Such a high spatial granularity will be critical to cope with the high particle occupancy for precision vertexing at future hadron colliders. Due to the severe confusion from overlapping particles, the tracking ability to reconstruct enormous number of particles produced in hadron collisions degrades quickly without a significant improvement in the timing capabilities of the detectors. It has been demonstrated by the LHC Collaborations that equipping HL-LHC experiments with 30 ps precision detectors would result in up to 20% improvement in the pileup vertices rejection factor [1, 2], which translates into a significant cost saving due to a reduced accelerator run-time. Precision timing together with spatial information will be critical not only to disentangle spatially overlapping or otherwise ambiguous events but also to identify the particles with different masses like K^+ mesons and π^+ mesons. In addition, precision time of flight measurements can be sensitive to the mass of heavy unknown charged particles, e.g. Dark Matter candidate, which typically have low β, speed relative to the speed of light.

The Low Gain Avalanche Diode (LGAD) technology is now a mature technology to achieve 30 ps

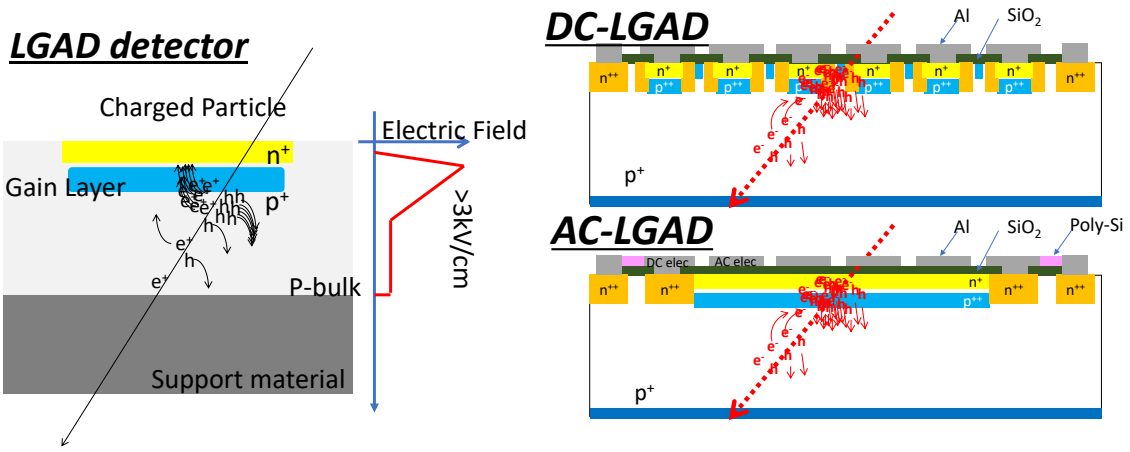

Fig. 1. Operation principle of the LGAD detector (left), and DC-LGAD and AC-LGAD detectors (right).

time resolution [3,4]. Figure 1 (left) shows the operation principle of the LGAD sensor. The LGAD is basically a n^+-in-p semiconductor diode, containing an additional p^{++} layer under the n^+ electrodes with a boron doping concentration larger compared to that in the p-bulk region. The additional layer makes an extremely higher electric field between n^+ and p^{++}. Such a high electric field induces avalanche multiplication, increasing the electron and hole pairs originally produced by a Minimum Ionizing Particle (MIP) by about 10-20 times. Superior time resolution is achievable with LGAD as such a large signal is produced in the vicinity of the depth region.

Concerning the spatial resolution, we have identified a potential issue in improving the granularity of the electrode [5]. Our fist segmented prototype, a 80 μm pitch strip detector, showed only 20 % of the region to have enough gain to achieve O(10) ps timing resolution. The reason of such a low fill factor is illustrated in Fig. 1 (top-right, DC-LGAD). The gain layers (combination of n^+ and p^{++}) are placed separately for each electrode. As the regions between the n^{++} electrodes have no gain, it introduces a gain non-uniformity over the sensor. To avoid this feature, an AC-coupled LGAD sensors (AC-LGAD) has been developed as described in Section 2.1. In the following sections, first HPK AC-LGAD prototype sensors are presented.

2. First prototype of AC-LGAD Sensors

2.1 Uniform avalanche layer and AC electrodes

To improve the active area with the high timing resolution, AC-LGAD sensors have been fabricated by HPK. A uniform gain layer (the set of n^+ and p^{++}) is placed over the sensor active area and for the segmented readout of the charge, patterned aluminum electrodes are placed on the oxide layer (AC-coupled to n^+) as shown in Fig. 1 (bottom right, AC-LGAD).

2.2 Parameterization of doping concentrations

A uniform gain layer with a low resistivity n^+ doping concentration is expected to result in large cross-talk to the next electrodes due to that the charge created by the avalanche point flows through the n^+ layer, creating signals on the neighboring electrodes. To reduce the cross-talk, an n^+ layer with large impedance is preferred. On the other hand, n^+ with such a lower doping concentration results in a lower gain. Therefore the p^{++} doping concentration must be optimized for each of the n^+ doping concentration. Table I summarizes the sample types produced in the first prototypes, with

seven variations in the concentrations.

Table I. The sample types produced as the first prototypes. In total seven types with three types of n^+ resistivity (A: DC-LGAD compatible, B: 3.3 times A, C: 10 times A) and three types of p^{++} doping concentration (1: low, 2: middle, 3:high) are produced. The samples corresponding to types C-3 and A-1 are not available as the early break down and lower gain, respectively.

		n^+ resistivity		
		C (A×10)	B (A×3.3)	A
p^{++} doping concentration	3 (high)	n/a	B-3	A-3
	2 (middle)	C-2	B-2	A-2
	1 (low)	C-1	B-1	n/a

The following three types in the electrode granularity have been fabricated.

- Pad type : 4 pads (2×2) with a 500 μm×500 μm pad size. Total size including periphery is 3 mm × 3 mm.
- Strip type : 48 strips with 80 μm pitch and 9880 μm long strip type electrodes. The width of strip electrode is varied, 30 μm, 35 μm, 40 μm and 45 μm. Total size including periphery is 12 mm × 6.7 mm.
- Pixel type : 196 pixels (14 × 14) with 50 μm×50 μm pixel type electrodes. The size of the pixel electrode is varied, 30 μm, 34 μm, 38 μm and 42 μm. Total size including periphery is 2.1 mm × 1.8 mm.

3. Performance measurements

This section describes the basic performance measurements and results. For the sensor operation, the reverse bias (negative voltage) is applied to the back side of the sensor and the n^+ layer is grounded via a poly-silicon resistor. In the later text reverse bias value is discussed as the absolute value of the negative voltage. The signal measurements were performed using a checking source with a scintillator trigger system.

3.1 Leakage current measurement (I-V)

To determine the operation voltage, breakdown voltages have been evaluated. Table II shows the breakdown voltage for each type of doping concentrations for the pad type sensors. The breakdown voltage ($V_{\rm bd}$) is defined by the bias where the leakage current increases more than double compared with the value at the bias 5V lower ($V_{\rm bd}$ − 5 V). The sensors with higher n^+ resistivity or the higher p^{++} doping concentration show a lower breakdown voltage as expected.

Table II. Measured breakdown voltage for each type of the pad sensors. See text for the definition of the breakdown voltage at 20°C.

		n^+ resistivity		
		C (A×10)	B (A×3.3)	A
p^{++} doping concentration	3 (high)	n/a	109 V	237 V
	2 (middle)	181 V	225 V	329 V
	1 (low)	279 V	311 V	n/a

3.2 Pulse height measurement setup

For the measurement of signal from the sensors, a fast amplifier and a high speed digitizer are used. The amplifier board is developed in 16 channel signal readout with two-stage charge amplifier integration circuits (IC) for each channel. The gain of the two-stage amplifier is approximately 100. The prototype sensors are mounted on an amplifier PCB by a conductive tape to apply the reverse bias from backside of sensor. The AC-LGAD readout electrodes are wire-bonded to the amplifier inputs. The amplified signals are extracted and digitized by a desktop digitizer, CAEN DT5742 (5 GHz sampling with 10-bit time memory and 12-bit ADC with 2 V full scale). A ^{90}Sr checking source place on top of was used to evaluate the sensor response to the minimum ionizing particles (MIPs). The pulse height signals are digitized on receiving an external trigger from a system consisting of a scintillator and two Multi-Pixel Photon Counters (MPPC) located under the amplifier board. Typical signal pulse shapes recorded by the digitizer are shown in Fig. 2. Three colored dotted curves correspond to the signal from the three electrodes of a pad sensor. The largest negative pulse (ch2, blue curve) is expected as the signal from the electrode where the beta-ray traversed (define this as the leading channel later in this text) and the other smaller pulses correspond to the cross-talk signals. The small positive overshoot observed for the leading pulse corresponds to the contribution where the induced charges flow away through the n^+ implant from the point beta-ray traversed. The pulse height is defined as the largest voltage among the sampling points with respect to the base line.

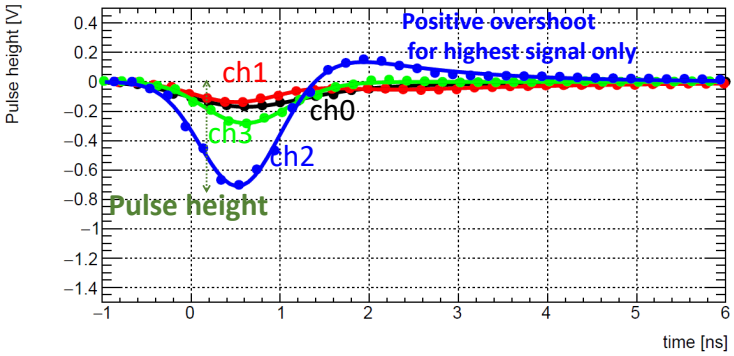

Fig. 2. Typical signal pulse shapes detected by a 4-channel pad sensor. Type C-2 at 180 V.

3.3 Pulse height analysis

The C-2 type described in section 2.2 is used for the pulse height analysis. The pulse height distribution, when applied with a 190 V bias voltage, as a function of the arrival time relative to the time of trigger is shown in Fig. 3 (top left). On-time events are defined as those in the region with a time difference less than 30 ns relative to the trigger. The events in the region with arrival time difference more than 40 ns and less than 100 ns are defined as off-time events. The off-time events are used to parametrize the pedestal distributions characterized by the intrinsic noise contributions from the sensor leakage current, the amplifier board and the digitizer. The distribution is fitted by an asymmetric Gaussian function as shown in Fig. 3 (bottom left) and sigma of right-tail Gaussian is used as the noise. Figure 3(middle) shows the distribution for the on-time events where curves fitted by a scaled pedestal function (blue) and a Landau distribution (red) as signal are overlaid. The most probable (MP) values of signal pulse height distributions and right tail sigmas of pedestal distributions are plotted as a function of the bias voltage in Fig. 3(right). A rapid increase in the pulse height was observed around the breakdown voltage (190V for C-2 type) and a noise increase starting at a voltage about a few ten volts higher than the breakdown voltage. So the optimal operation region of the device

can be determined to be ±20 V around breakdown voltage. The pulse height distribution in the region where the noise increases may not allow a proper evaluation as difficulty in separation of the signal and noise.

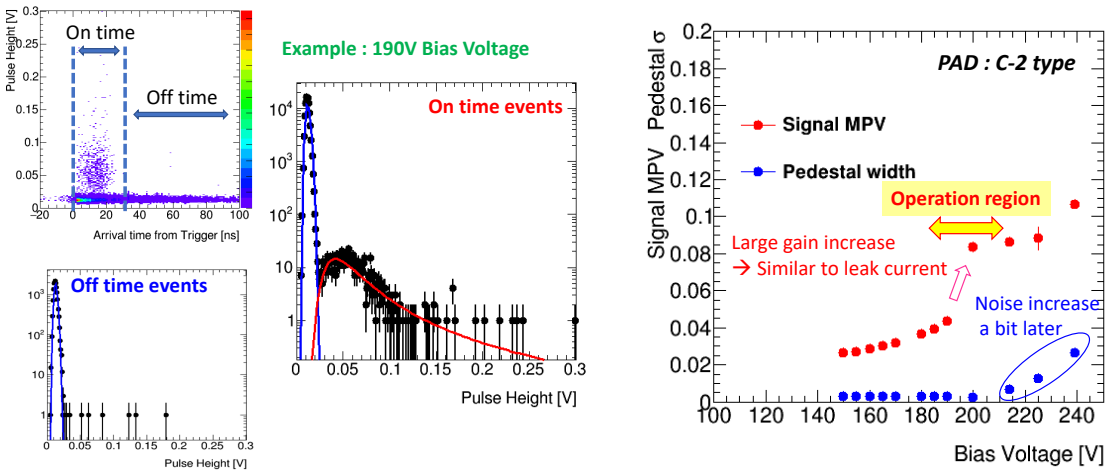

Fig. 3. Pulse height distributions for on-time and off-time events (see text), and signal and noise voltages as a function of bias voltage.

3.3.1 Signal cross-talk

The most important issue in designing an AC-LGAD sensor is whether the cross-talk can be reduced. The amount of cross-talk was measured by the pad type and strip type sensors as shown in Fig. 4. The electrode with the highest pulse height in an event was defined as the leading electrode and the pulse height ratios were defined as the other pulse heights relative to that in the leading electrode. The results for type A-3 and C-2 pad sensor samples are compared in Fig. 4 (top left) and (bottom left), respectively. The blue and green curves are pulse height ratios corresponding to the pad at diagonal and to the two pads sharing the same side with the leading pad, respectively. The C-2 type shows a smaller cross-talk (20%) while a larger cross-talk is observed in A-3 type (more than 70%). This indicates that AC-LGAD must have a sufficiently higher n^+ resistivity to suppress the cross-talk. For the strip sensor, the pulse height ratios were plotted as a function of the distance from leading strip in a unit of number of strips, as shown in Figure 4 (right). The cross-talk to the next strip is 75% and next-to-next strip is 62%.

Only 20% of cross-talk was observed for the pad of 500 μm width, while the cross-talk at the position 6 strips away from the leading electrode (480 μm) is 45 % for the strip. We observed that the strip sensor has a larger cross-talk compared to the pad sensor. This feature will be discussed in Section 4.

3.3.2 The signal size comparison between pad and strip sensors

As the AC-LGAD sensor is designed with the signal readout via the capacitive coupling electrode, the signal size should depend on the coupling capacitance (C_{cp}) of the readout electrode. To check the dependence, the signals from the pad sensor and strip sensor are compared at the same bias as shown in Fig. 5. As can be seen, the pad sensor has a signal 3.9 times larger than strip sensor signal while the effective coupling capacitance value of pad is larger than strip sensor. The relationship between the signal size and coupling capacitance will be discussed in Section 4.

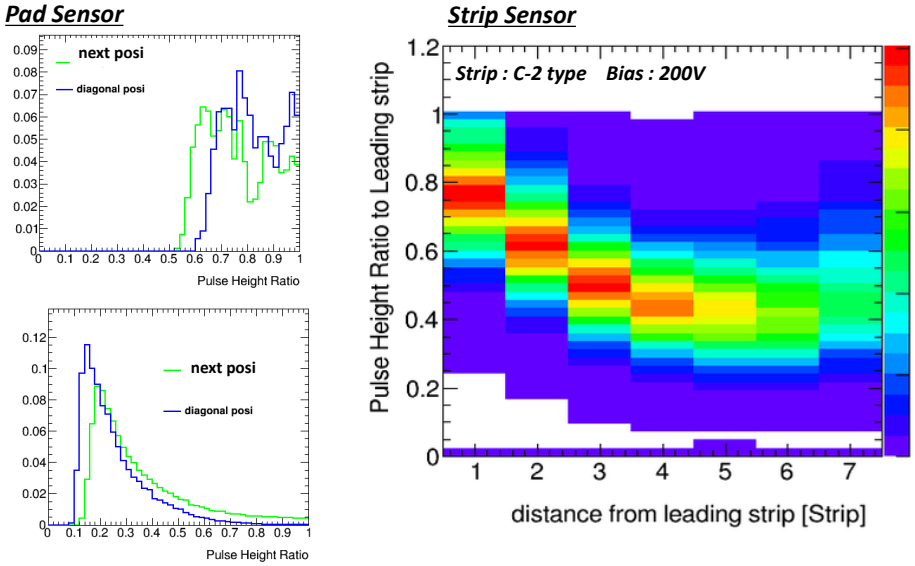

Fig. 4. The size of cross-talk for pad (left) and strip (right) type sensors. The pulse height ratios to the highest signal are plotted for A-3 type (top left) and C-2 type (bottom left). The pulse height ratios as a function of the distance in unit of number of strips are shown in right for C-2 type strip sensor.

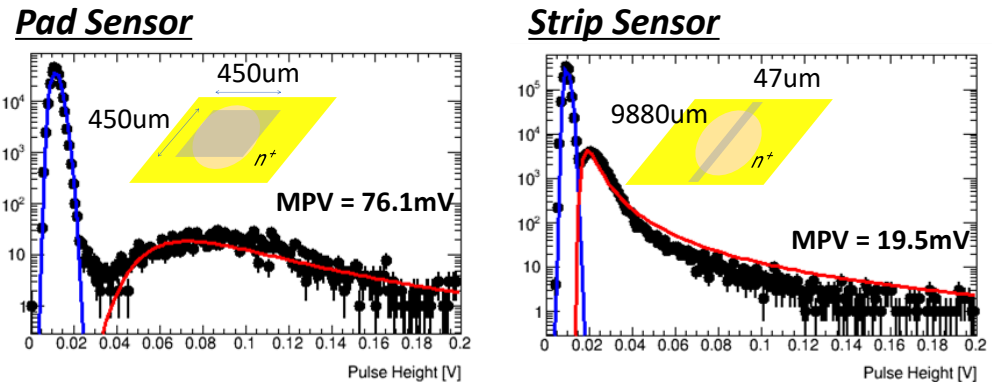

Fig. 5. Signal size comparison between the pad sensor (left) and strip sensor (right) at the same bias voltage.

3.3.3 Timing resolution

The timing resolution of the AC-LGAD sensor is discussed as it is an important performance for the LGAD sensors. To evaluate the timing resolution, two of type C-2 pad sensors are stacked with about 1 mm space between the two sensors. The pulse height distributions from 8 electrodes (4 electrodes per pad sensor) are analysed. Figure 6 (left) shows a typical pulse height distribution, showing that the signal (red Landau) is well separated from the intrinsic noise (blue). The standard deviation of the arrival time differences from the two stacked sensors ($\sigma_{T_1-T_2}$) can be expressed as in Equation 4.

$$\sigma_{T_1-T_2} = \sqrt{(\sigma_1)^2 + (\sigma_2)^2}, \tag{1}$$

where σ_1 and σ_2 are the timing resolutions of first and second sensors, respectively. In case the same type of sensors are stacked, as the timing resolutions of first and second sensors are expected to be identical ($\sigma = \sigma_1 = \sigma_2$), the timing resolution of a single sensor can be determined by Equation 2.

$$\sigma = \sigma_{T_1 - T_2} \times \sqrt{2}. \tag{2}$$

The arrival time differences between the two stacked sensors are shown in Fig. 6 (middle). As the distributions include contributions by different signal routing on the printed circuit board and digitizer channels, all 16 combinations out of two 4-pad sensors are separately calibrated for such differences. The corrected timing resolution as a function of the threshold to the signal pulse height is shown in Fig. 6 (right). The threshold to keep a 99% efficiency for the signal is chosen to determine the timing resolution. The evaluated timing resolution is 45 ps.

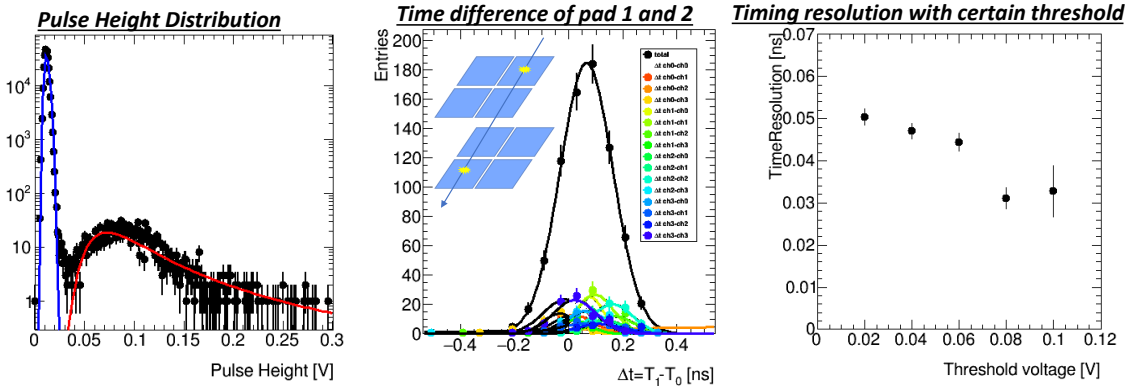

Fig. 6. Timing resolution of a C-2 pad sensor. Signal pulse height distribution (left), timing differences between the two stacked sensors (middle) and the evaluated timing resolution (right) as a function of threshold to the signal pulse height.

4. Summary and discussions

4.1 Summary of the results

First HPK AC-LGAD prototypes produced in seven sample types of different n^+ and p^{++} doping concentrations have been characterized for their basic performance. The leakage current was measured to obtain the breakdown voltage for each type of the sensors. The C-2 type is found to have a lowest cross-talk and highest gain showing a breakdown voltage at 190 V. The pulse height has been analyzed to observe the gain to increase around the breakdown voltage while the noise to increase at a voltage 30 V higher than the breakdown voltage. For the cross-talk, we observed about 20% for the pad type sensor, and 75% and 68% in the strip type sensor to the next and to next-next strip, respectively. An interesting observation is that about 45% cross-talk at the position 6 strip away (480 μm) for the strip sensor, while about 20 % for the pad sensor with 500 μm pad width. There is a significant pulse height difference between the pad and strip sensors; The pad sensor has a pulse height 3.9 times larger than the strip sensor at the same bias voltage. This indicates that the pulse height is dependent on the coupling capacitance between readout aluminum and the n^+ implant layer. The timing resolution was measured and we obtained a 45 ps resolution with a 99% of signal efficiency.

4.2 Discussions

Figure 7 illustrates that the charge produced by the avalanche (Q_0) flows in two directions, one is read out via capacitive coupling (C_{cp}), and the other is cross-talk through the n^+ implant with an effective resistance (R_{imp}). The pulse height size is determined by the two components, $Z_{C_{cp}}$ and $Z_{R_{imp}}$ which are the impedance of C_{cp} and R_{imp}, respectively. So the charge read out to the amplifier (Q) is determined by the following equation,

$$Q = \frac{Z_{R_{imp}}}{Z_{C_{cp}} + Z_{R_{imp}}} \times Q_0. \tag{3}$$

$$Q = \frac{R_{imp}}{1/(2\pi f C_{cp}) + R_{imp}} \times Q_0, \tag{4}$$

where f is effective frequency of the pulse signal. The larger C_{cp} and higher R_{imp} results in a higher pulse height signal and lower cross-talk ($Q_0 - Q$). This model can describe the observed characteristics at least qualitatively described in Section 3.3.1 and 3.3.2. The geometrical coupling capacitance per readout channel is twice larger for the strip sensors than for the pad sensors. However, the effective coupling capacitance should be dependent on the resistivity of the n^+ implant, e.g. limited area about the avalanche point is contributing to the effective capacitance. This feature results in a smaller signal size and larger cross-talk in the strip sensors compared to the pad sensors. This model will be tested more systematical way by producing other sensors in the next fabrication with higher n^+ implant resistivities and thinner oxide layer thicknesses.

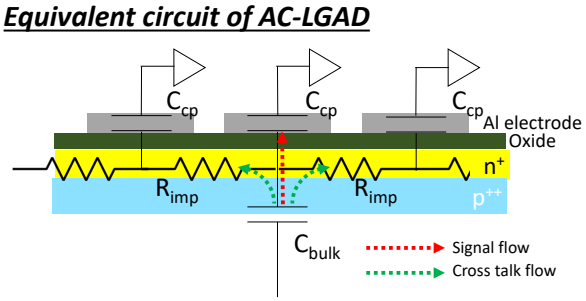

Fig. 7. Equivalent circuit of the AC-LGAD sensor. Signal flow and cross-talk flow are shown by red and green dotted arrows.

5. Conclusions

In conclusion, the fist HPK AC-LGAD sensors show an expected performance for 500 μm $\times$ 500 μm pad sensors and 80 μm pitch strip sensors. With the present strip sensor, we expect a 23 μm spatial resolution assuming digital readout, with reasonably small cross-talk. Further optimization of n^+ and p^{++} doping concentrations is necessary for smaller electrode sensors, like pixel sensors. Increasing the n^+ implant resistivity will help improve the lower signal in such devices.

Acknowledgments

This research was partially supported by Grant-in-Aid for scientific research on advanced basic research (Grant No. 19H05193 and 19H04393) from the Ministry of Education, Culture, Sports,

Science and Technology, of Japan as well as the Proposals for the U.S.-Japan Science and Technology Cooperation Program in High Energy Physics for JFY2019 granted by High Energy Accelerator Research Organization (KEK) and Fermi National Accelerator laboratory (FNAL). In keeping the research program move forward, the following two facilities were very important to this project : Cyclotron Radio Isotope Center (CYRIC) at Tohoku University and Fermilab Test Beam Facility (FTBF) at Fermi National Accelerator Laboratory (FNAL).

References

[1] Technical Design Report: A High-Granularity Timing Detector for the ATLAS Phase-II Upgrade "CERN-LHCC-2020-007 ; ATLAS-TDR-031"
[2] Layout and performance of HPK prototype LGAD sensors for the High-Granularity Timing Detector "Nuclear Instruments and Methods in Physics Research Section A: Accelerators, Spectrometers, Detectors and Associated Equipment" Volume 979, 1 November 2020, 164382
[3] Evaluation of characteristics of Hamamatsu low-gain avalanche detectors, S. Wada, K. Hara, K. Nakamura, "Nucl. Instrum. Methods Phys. Res., Sect. A", PoS (VERTEX2019)057 Mar 2020.
[4] Layout and performance of HPK prototype LGAD sensors for the High-Granularity Timing Detector " Nuclear Instruments and Methods in Physics Research Section A: Accelerators, Spectrometers, Detectors and Associated Equipment" Volume 980, 11 November 2020, 164379.
[5] Study of time resolution of low-gain avalanche detectors, K.Onaru, K. Hara, D Harada, S. Wada, K.Nakamur, Y.Unno, "Nucl. Instrum. Methods Phys. Res., Sect. A", Volume 985, 1 January 2021, 164664